AUTHOR'S POST PRINT (Romeo Colour: Green)
MSSU: Microgravity & Space Station Utilization (ISSN: 0958-5036), 3(4): 39-49 (2002).
Publisher version available at
http://www.liguori.it/periodici.asp?cod_collana=201

THE FLUID-DYNAMICS OF THE ISS MICE DRAWER SYSTEM UNDER MICROGRAVITY

M. Lappa[*], D. Castagnolo[*], A. Sgambati[+]

[*]MARS (Microgravity Advanced Research and Support Center) Via Gianturco 31 - 80146, Napoli, Italy,
[*]current e-mail address: marcello.lappa@strath.ac.uk
[+]Laben (Laben S.p.a., Strada Padana superiore 290, 20090 Vimodrone, Milano, Italy)

Abstract - The present paper deals with the "critical analysis" of the environment that will be provided by the MDS (Mice Drawer System) under microgravity conditions. This system will be used to study the "extended" growth and life of mice on the International Space Station (ISS). A very long period (100 days) will be investigated taking advantage of the availability of the ISS platform. The complex physical-chemical system (fluid-dynamics, ventilation, air-conditioning, oxygen and carbon dioxide levels and distributions, etc.) that will be established in absence of gravity inside the MDS is simulated through solution of a custom system of partial differential equations. The choice of custom model is motivated by the advantage to insert boundary conditions and complex equations that provide a clear understanding of the phenomena involved and a wide spectrum information to match the requirements for the maintenance and the well-being of the animals.

1. INTRODUCTION

Many shuttle missions have carried scientific experiments involving animals, from rats and mice to bees and jellyfish. The experiments have been used to test the effects of microgravity and other conditions in space on how animals behave, grow, and reproduce in this altered environment [1,2]. These experiments allowed the investigators to attribute many of the observed adaptive cardiovascular, musculoskeletal, and neurovestibular changes to the microgravity exposure. Moreover a secondary focus of ongoing animal investigations is to determine how gravitational inputs modulate the complex regulatory mechanisms that may be involved in Earth-based diseases such as anemia, osteoporosis, muscular atrophy, and immune system dysfunction. Animal studies in space are very conducive to the understanding of the effect of microgravity conditions as well as (by comparison) of the effect of normal gravity conditions on the life and on the disease and dysfunctions of living organisms. This has led to important results in the framework of bone (see, e.g., [3-6]), muscle and neuro-sensory physiology and of many other biological sciences.
Note that many of the experiments carried out today use rodent payloads that are transported into space aboard the space shuttle. This choice is motivated by the necessity to limit the dimensions as well as the weight of such payloads (mice are small creatures) and by the fact that such animals have been proved to be a good surrogate to test and to discern physiological microgravity effects (they allow to develop and test concepts that can be extended to the human case).
The use of rodents for physiological investigations has been also highlighted recently by the Microgravity Advisory Committee (MAC) and documented in the last "Approach to Microgravity Follow-On Program" issued by the ESA Microgravity Program Board (Cotronei et al. [7]). This emerging need has led to the design and development of the Mice Drawer System (MDS) facility which makes it possible the execution of experiments using mice as models for human physiology.
It is worthwhile to point out how taking animals into space however requires special considerations. NASA maintains the highest standards for the humane care and treatment of its laboratory animals. In addition to complying with all applicable regulations and guidelines, the agency has internal policies that govern the care and use of research animals for all activities, including activities at foreign institutions.
Along these lines, the present paper deals with the fluid-dynamic analysis and the "critical design" of the environment that will be provided to mice by the aforementioned MDS facility. This system will be used to investigate the "extended" growth and life of mice on the International Space Station (ISS), which allows experimentation for a very long period (100 days).
Note that the term "environment" is here used to denote the complex physical-chemical system (atmosphere, fluid-dynamics, ventilation, air-conditioning, oxygen and carbon dioxide levels and distributions, etc.) that will be established inside the MDS. Many environmental influences have to be taken into account to guarantee a proper environment for the growth and life of the mice.

2. THE MICE DRAWER SYSTEM

The MDS can be thought of as a miniature laboratory animal facility in the sense that it contains all of the components that are required for maintenance of the animals during a mission. The related design has been developed by Laben S.p.a. and supported by the Italian Space Agency (ASI). Scope of MDS is to provide a

general purpose facility to be used by a large number of researchers and scientists for different experiment types. Therefore, the whole facility and every included subsystem, has been conceived in such a way as to provide a high degree of flexibility.

Food and water consumption can be monitored, and the water reservoir bags can be refilled during the flight as required. On-orbit access to animals, active temperature control, video monitoring, and food and water replenishment are incorporated in such hardware.

The Observation Subsystem permits the observation of mice through a video camera. Video data can be transmitted to ground in order to permit a near real-time verification of mice health status and behavior.

The MDS Mice Chamber is divided in two different habitats composed by 3 equal compartments, each one able to host one mouse, so that each mouse can be kept separate inside a dedicated and isolated cage (Figs.1).

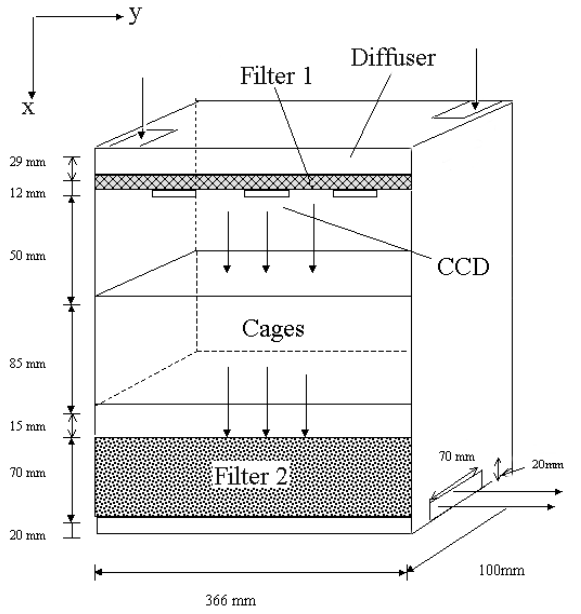

(a)

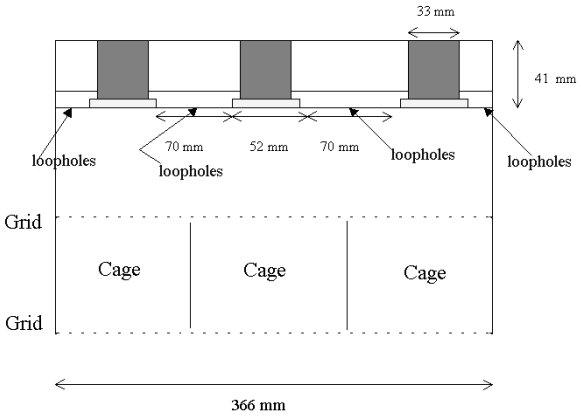

(b)

Figure 1: Sketches of the MDS system: (a) full view, (b) details of the diffuser and the cage region.

This has a twofold purpose:

- to prevent any physical interaction and reduce biological contamination among mice
- to permit the execution of six experiments in parallel (one for each mouse independently)

The Air Conditioning Subsystems represents one of the most critical subsystem of the facility since mice health status and well-being depends mainly on its proper operation.

Main tasks performed by the Air Conditioning Subsystem are:

1) to provide mice with needed air ventilation. i.e. to control the oxygen and carbon dioxide levels inside the mice chamber. Note that this is obtained by exchanging air with the ISS cabin. The air exchanged with the cabin is only the percentage needed for mice ventilation while remaining air is internally recycled.

2) to remove waste products from the cages.

3) to filter air exchanged with the cabin in order to prevent airborne cross-contamination between the cabin and MDS internal air (in both directions); to filter air ejected to the cabin in order to remove odors; to filter internally recycled air in order to reduce airborne cross-contamination between mice.

Each cage has two sides open in order to permit the air to flow through. The direction of this flow, which simulates a low gravity effect, permits the identification of the cage floor (or bottom side) which results to be the side in contact with filters and parallel to the MDS Front Panel.

The following measures for a cage, each one able to host one mouse, have been defined:

125 x 100 x 85 [mm] (W x D x H)

Cages have been oriented in such a way that the air flows through the two 125 x 100 [mm] sides (see Figs.1).

Air circulation is accomplished by a system of fans that pull air to the back of the cage and through a high efficiency particulate air (HEPA)/charcoal filter and into the animal quarters. After the air passes through the cage, it traverses a second filter where all particulate matter and odors are removed before the air is returned to the orbiter cabin and/or internally recycled (Fig.1a).

Air is injected into the Mice chamber through a diffuser (see in particular Fig. 1b), which represents one of the most critical subsystem of the facility. The diffuser collects the volumetric rates internally recycled $\dot{m}_{fan}$ (needed to provide a suitable velocity inside the mice chamber to remove the cage from waste products) and externally coming from the ISS cabin $\dot{m}_{ISS}$ (needed to restore the normal oxygen and carbon dioxide levels). The ultimate aim of the diffuser is to provide an air flow in the mice chamber as close as possible to uniform and laminar conditions. The cylindrical bodies of the videocameras needed for mice observation are embedded in the inner space of the diffuser leading to a very complex geometry (Fig. 1b). For this reason the design of the diffuser is a "key parameter" of the overall system as well as a crucial factor for making it a proper environment.

3. THE BALANCE EQUATIONS

For the problem under investigation (see also Refs. [8-13]) fluid motion and associated transport of gases (oxygen, carbon dioxide, etc.) are governed by the Navier Stokes equations and by the corresponding species transport equations:

$$\underline{\nabla} \cdot \underline{V} = 0 \qquad \textit{(continuity)} \qquad (1)$$

$$\frac{\partial(\underline{V})}{\partial t} = -\frac{1}{\rho}\underline{\nabla} p - \underline{\nabla} \cdot [\underline{V}\underline{V}] + \nu \underline{\nabla} \cdot [\underline{\nabla} \underline{V}] - \frac{1}{\rho} A \, \underline{V}$$

(momentum) (2)

$$\frac{\partial C_i}{\partial t} = \left[-\underline{\nabla} \cdot (\underline{V} C_i) + D_i \nabla^2 C_i \right] + \dot{C}_i$$

(species) (3)

Equations (1-3) represent a set of differential partial equations of parabolic-hyperbolic nature with respect to space and time. The above set has been solved in the complete form (three-dimensional, non-linear and time-dependent) without any simplifying assumption. In the equations (1-3) , $\underline{\nabla}$ is the gradient operator, ∇^2 the Laplacian, $\underline{V}$ the velocity vector, p the pressure, t the time, ν the kinematic viscosity [cm^2/s], ρ the density [g/cm^3], C_i the concentration of the specie ($i = O_2, CO_2$), D_i and $\dot{C}_i$ the associated diffusion coefficient and the rate of production, respectively. The constant A in eq. (2) is the constant of proportionality between the volumetric flow rate Q and the pressure decrease Δp through porous filters present in the computational domain (i.e. $Q = -A^{-1} S \frac{\Delta p}{l}$ where S and l are the area and the thickness of the porous filter, respectively); its value is set equal to zero in regions where filters are absent.

Every thermofluid-dynamic property can be considered constant. Chemical reactions and dissociation phenomena are supposed to be absent.

It is noteworthy how for the MDS system under microgravity conditions, fluid motion is due only to "forced convection" (provided by the aforementioned Air Conditioning Subsystem). Natural convection caused by buoyancy forces and density gradients is absent or negligible (due to the reduced gravity environment). Consequently the Boussinesque source term in the momentum equation responsible for buoyancy-induced-flows is not taken into account.

4. THE NUMERICAL METHOD

The set of equations (1-3) under the initial and the boundary conditions are solved numerically in a Cartesian frame of reference in primitive variables by means of a control volume method. The domain is discretized with a uniform and structured mesh and the flow field variables defined over staggered nodes.

The velocity component V_Z is staggered in the z direction with respect to the point in which pressure is computed. In a similar way the other velocity components V_X and V_Y are staggered along the x and y directions, respectively.

The finite volume approach relies directly on the application of the integral form of balance laws. Thus the conservation laws are written for an arbitrary spatial domain Ω bounded by a surface $\partial\Omega$. Since the collocation of the variables on the mesh is staggered, a different control volume characterizes each variable.

The problem is solved with the well-known Marker and Cell method (see, e.g., Harlow and Welch [14]). The computation of the velocity field at each time step is split into two substeps.

In the first, an approximate non-solenoidal velocity field $\underline{V}^*$ which corresponds to the correct vorticity of the field is computed at time (n+1) neglecting the pressure gradient term in the momentum equation (2). In the second substep, the pressure field is computed by solving the equation resulting from the divergence of the momentum equation taking into account eq. (1):

$$\nabla^2 p^n = \frac{1}{\Delta t} \underline{\nabla} \cdot \underline{V}^* \qquad (4)$$

This equation is solved with a SOR (Successive Over Relaxation) iterative method.

Finally, the correct solenoidal velocity field is updated using the computed pressure field to account for continuity:

$$\underline{V}^{n+1} = \underline{V}^* - \Delta t \underline{\nabla} p^n \qquad (5)$$

The modeling of the filters follows the excellent ideas and concepts pointed out in the works of Voller and Prakash [15], Bennon and Incropera [16], Brent et al. [17].

The subroutines for the above computations have been widely validated during the last ten years at MARS Center; references [18-20] report benchmarks of various transport phenomena, where the model has been applied successfully. Very dense computational meshes (see Table I) have been used for the simulations ($O(10^6)$ points). Table II shows the properties of the impurities and of air and the operating conditions used for the simulations.

5. THE DIFFUSER

It is important to point out how the diffuser design is the results of a trade off between volume available and flow requirements.

A system of loopholes uniformly distributed along y and along z has been used to characterize the outflow section (Figs.2). Each loophole has Diameter = 2 [mm]. The distance between the center of two consecutive loopholes (along y or along z) is equal to 3.5 [mm] (see Fig. 2b).

Note that the loopholes have been uniformly placed around the cameras with the exception of the areas corresponding to the inflow sections located on the back of the diffuser (Fig.2a). This artifice is used to avoid the very large flow velocities that otherwise would occur in these zones due to the perpendicular flow entering the diffuser from the back side. According to the above arguments a pattern of 2152 loopholes has been obtained (Fig. 2c).

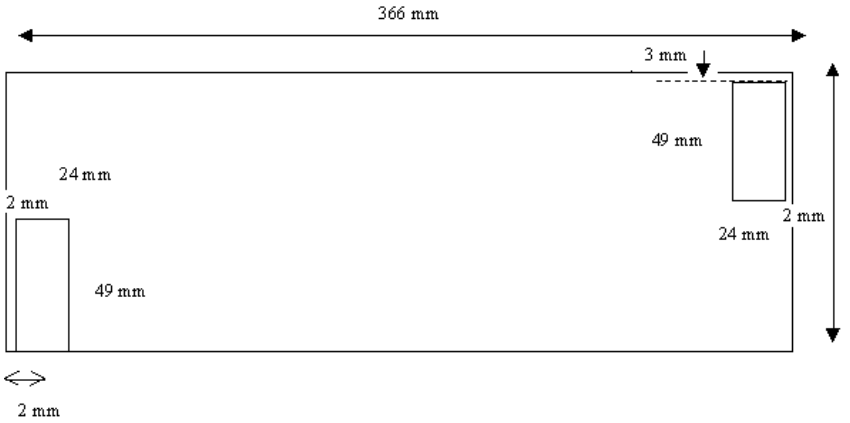

a)

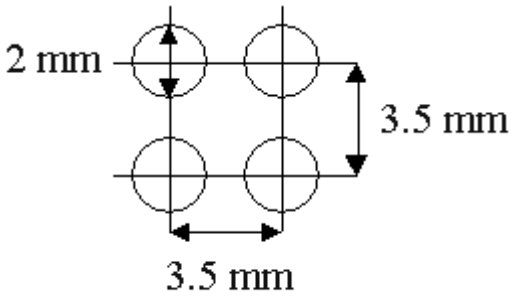

b)

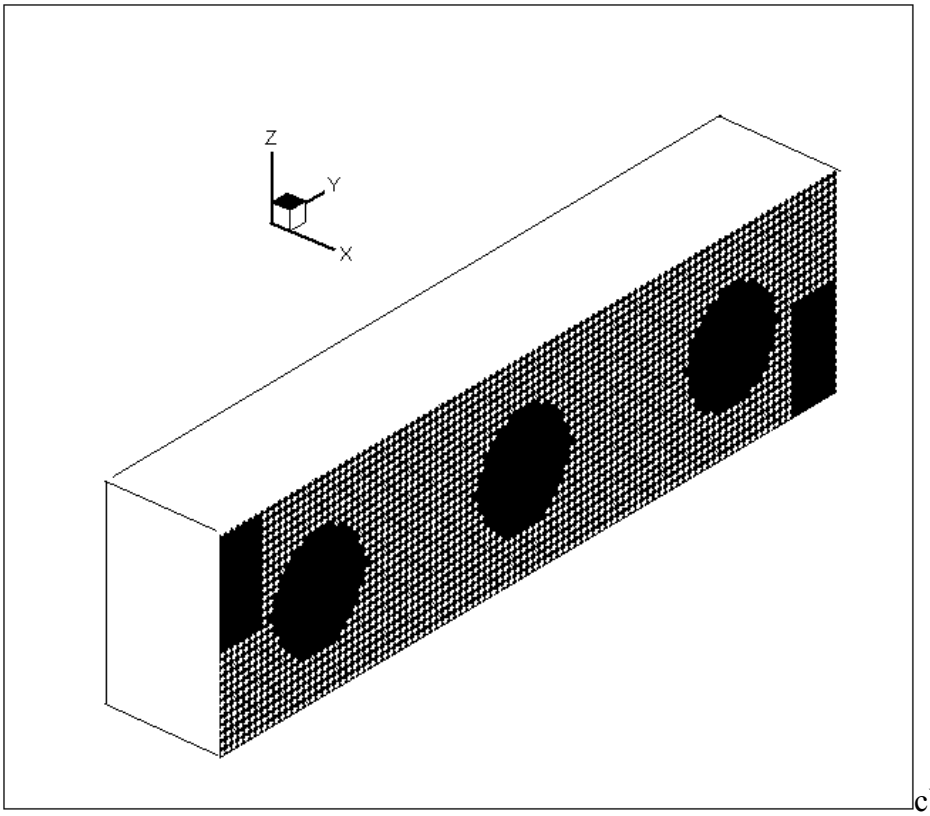

c)

Figure 2: a) Back view and inflow sections for the diffuser,
b) loopholes configuration
c) Sketch of the outgoing section (front view) of the diffuser and related pattern of loopholes

The cylindrical bodies of the video cameras inside the diffuser have been taken into account using a VOF technique (Volume of Fluid Method, Hirt and Nichols [21], Gueyffier et al. [22]) that allows one to undertake a fixed-mesh solution and therefore to utilize standard solution procedures for the fluid flow and species equations directly, without resorting to mathematical manipulations and transformations.
The simulations have shown that the presence of these cylindrical bodies is crucial in determining the structure of the flow field inside the diffuser and therefore the behavior of the exiting flow in terms of direction and intensity distribution.

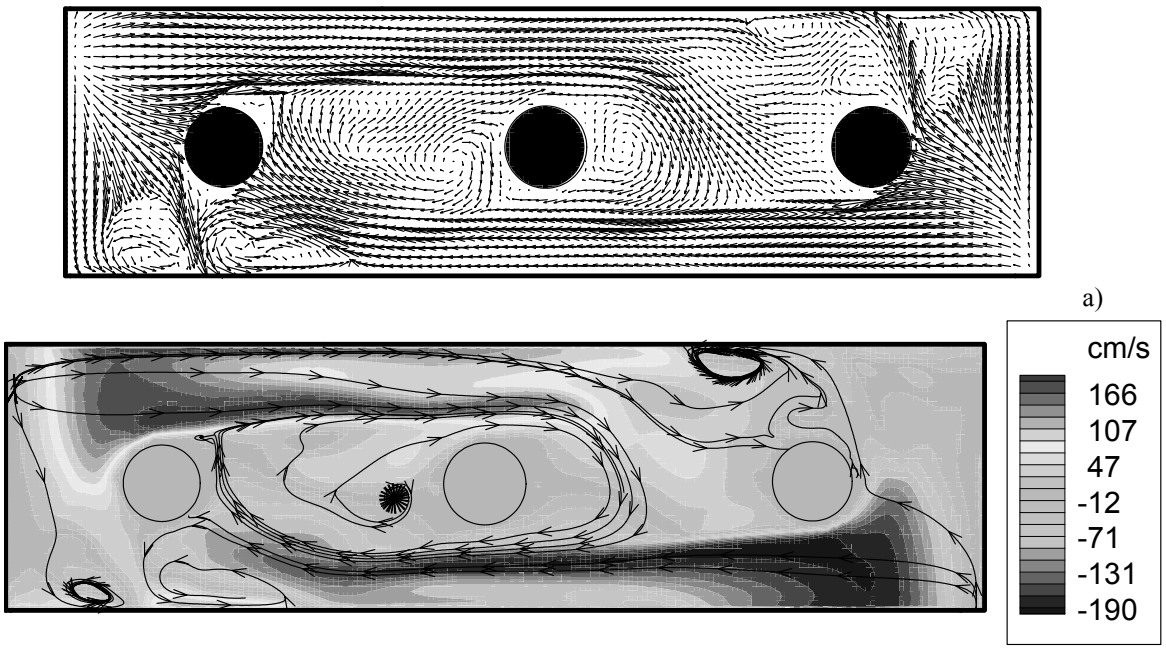

Figures 3:

a) Vector plot of the flow field inside the diffuser,

b) contour map of the velocity component along y in the midsection

The fluid enters the diffuser from the back side directed along x. Because of the geometrical constraints (the outflow section of the diffuser does not have holes on the regions corresponding to the back inflow sections), the fluid has to turn to flow along y. The resulting two main flows have similar form but are directed in the opposite directions (see Figs.3, hereafter, for the sake of brevity, the camera located at y=0 will be referred to as the "central" camera whereas the others as the "lateral" cameras).
Note that the aforementioned effect leads to the formation of two "fingers" wrapped around the body of the central camera. These "fingers" are high velocity elongated regions produced by the cross-sectional area contraction encountered by the fluid moving along y due to the presence of the cylindrical bodies of the cameras embedded in the inner space of the diffuser.
Due to the interplay and mutual interaction occurring between these two opposite flows, a very complex "multicellular" pattern arises (see Fig. 3a). Some vortices are formed among the central camera and the lateral ones. The main structure of the velocity field consists of some trajectories "wrapped" around the central camera. At the same time two secondary small rolls are created, the first located below the first camera and the second located above the third camera (see Figs. 3a,b). Of course the flow does not exhibit mirror symmetry with respect to the midplane z=0. This behavior follows from the position of the inflow sections on the back of the diffuser (see Fig. 2a). It is very important to stress how the flow is not symmetric by reflection also with respect to the midplane along y (y=0 [cm]). The fluid particles trajectories in fact cross this plane directed along the positive (negative) y direction above (below) the central camera.
One must keep in mind however that a flow motion along x (Fig. 4) is superimposed on these behaviors. The velocity component along x ranges from 0 to 33 [cm/s] and the related maxima are located in the regions surrounding the rectangular areas of the diffuser outflow section without holes (located at the same height and position of the back inflow sections).

For this reason, some effort is devoted to point out such structure.
Since the flow field is three-dimensional in nature, a detailed description of the behavior needs separating the analysis for the different directions. First the attention is focused on how the fluid motion behaves along y, then the behavior along x is taken into account.
Figures 3a,b show that a complex flow field is established inside the diffuser. It follows from the interaction of the flow entering from the back sections with the cylindrical bodies embedded in the inner space of the diffuser.

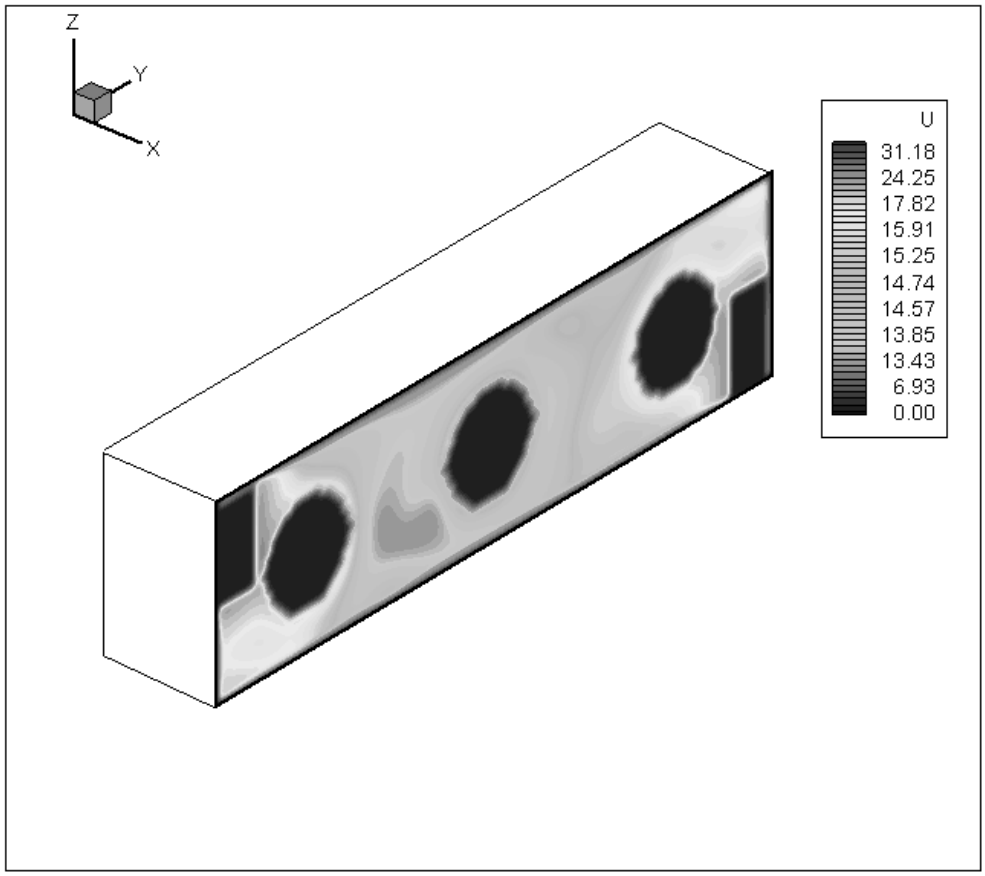

figure 4 x-component of the velocity at exit from diffuser, units in cm/s.

It is worthwhile to stress how the flow exiting the diffuser is almost parallel to the x axis whereas the velocity components along y and z are small. This feature is very important since it matches the requirements. A parallel flow turns out to be crucial for the structure of the flow field in the cages system. The pattern of loopholes selected in the present study seems to be a very suitable condition for achieving an almost parallel and uniform flow through the cages system (further details on this topic will be discussed in the next section).

6. THE CAGE SYSTEM

The flow distribution and some trajectories are illustrated in Figures 5 in planes cutting the whole system at z=4 [cm] and z= 0 [cm] respectively.
It is evident that the streamlines are almost parallel and the flow is almost uniform through the cages. The average velocity is about 10 [cm/s].
It is interesting to point out how close to the outgoing section of the diffuser however the flow in nor uniform neither parallel to the x axis. Since the regions corresponding to the presence of the cameras do not have holes, there the fluid tends to recirculate leading to the onset of local roll structures where the fluid is close to stagnation conditions. Such vortical structures however have a very small size. They are confined to the regions located between the outgoing section of the diffuser and the cages. Their effect on the direction of the flow in the cages can be considered almost negligible.
Behind the cages the flow is strongly curved since it enters the cages ambient with a velocity component along x and then it is forced to leave the system through outgoing sections located on the lateral walls (the outflow sections are located in the corners and for this reason the flow has to turn of almost 90 degrees). This feature however is not crucial for the system under investigation since the direction of the flow behind the cages is not important for the purpose of MDS.
Note that the presence of the mice cage grids has also been taken into account for the numerical simulations. However their overall effect seems to be almost negligible.
On the contrary, the presence of walls separating the cages cannot be ignored. Fortunately they have a very beneficial effect on the flow. Such walls oriented along x in fact represent a further beneficial constriction for the fluid leading to parallel streamlines through the cages.
Figs. 5b shows that the velocity in the midplane z=0, tends to be larger in the lateral cages (V≅15 [cm/s]) than in the central cage (V≅10 [cm/s]). This is due to the very decentralized positions of the diffuser's back inflow sections that drive high velocity fluid in the diffuser close to the lateral walls, leading, as already discussed in section 5, to larger outflow velocities close to the lateral cameras (see Fig. 4).

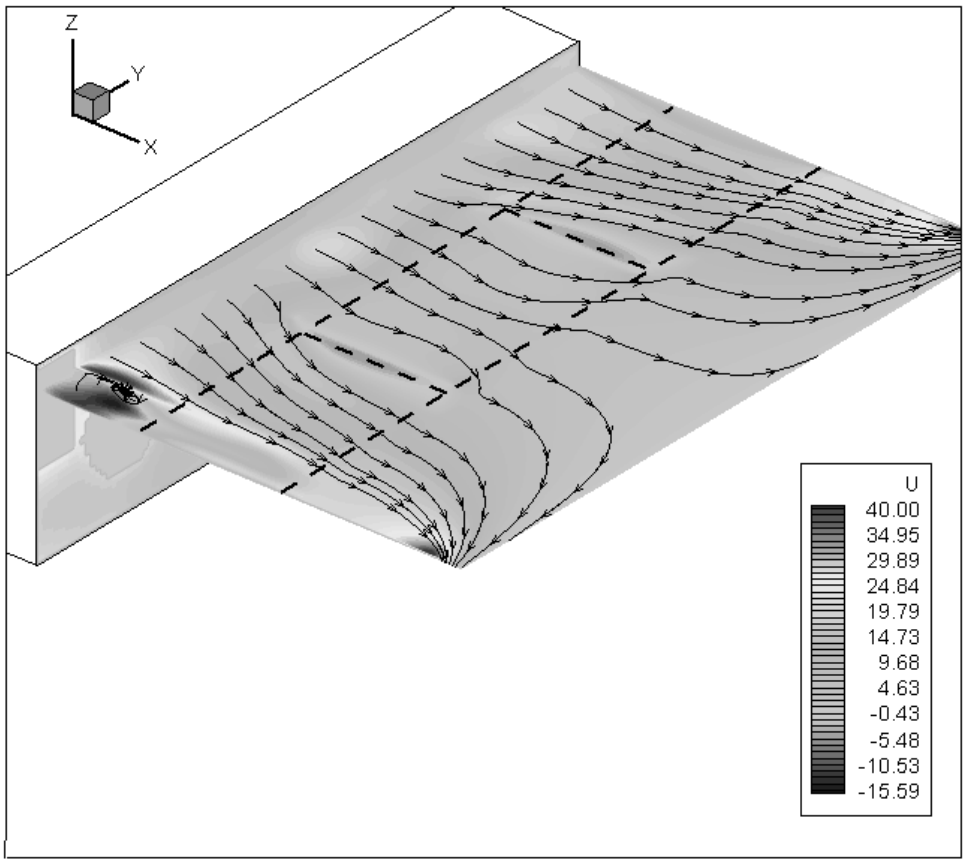

figure 5a: flow in the plane z=4 [cm], U is the component of the velocity along x, units are in cm/s.

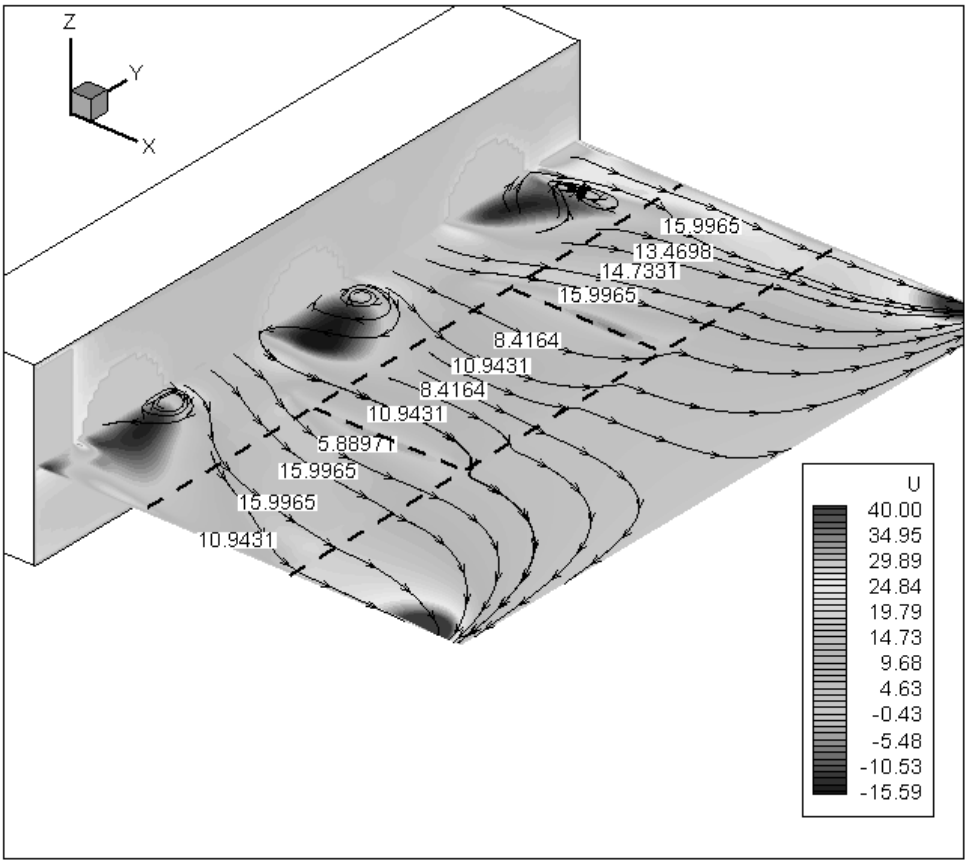

figure 5b: flow in the plane z=0 [cm] (midplane), U is the component of the velocity along x, units are in cm/s.

Despite the presence of (a) vortical structures at z=0 near the diffuser outflow section, (b) larger outflow velocities close to the lateral cameras, and (c) a very curved flow behind the cages, the flow through the cages is almost parallel and uniform. The deviations (a),(b),(c) with respect to an "ideal" perfect parallel and uniform flow are tolerable and do not significantly alter the behavior of the system under investigation with respect to the "ideal" condition. Moreover a very suitable degree of transport and removal of the impurities and toxic gases is achieved (see below).

The concentration of the incoming flow (C^{in}) is computed as function of the concentration of the outgoing flow and of the concentration of the cabin air (e.g. in the case of carbon dioxide it is 0.7%). The incoming volumetric flow rate in fact (see section 2) is the sum of two contributions: $\dot{m}_{fan}$ is a volumetric flow rate associated with the recirculating air, $\dot{m}_{ISS}$ is a volumetric flow rate coming from the cabin in order to maintain an acceptable concentration of oxygen for the mice; the concentration associated with $\dot{m}_{fan}$ is equal to the concentration obtained at the outgoing section of the cage ambient C^{out}, whereas the concentration associated with $\dot{m}_{ISS}$ is equal to a constant value C^{ISS}.

$$C_{CO_2}^{in} = \frac{\dot{m}_{fan} C_{CO_2}^{out} + \dot{m}_{ISS} C_{CO_2}^{ISS}}{\dot{m}_{fan} + \dot{m}_{ISS}} \qquad (6)$$

Since there is a mice carbon dioxide production (24400 [ml/day]) the foregoing equation leads to an iterative procedure in time (see Fig.6) where C^{in} and C^{out} change with time but after a certain transient time period, a steady regime shall be reached.

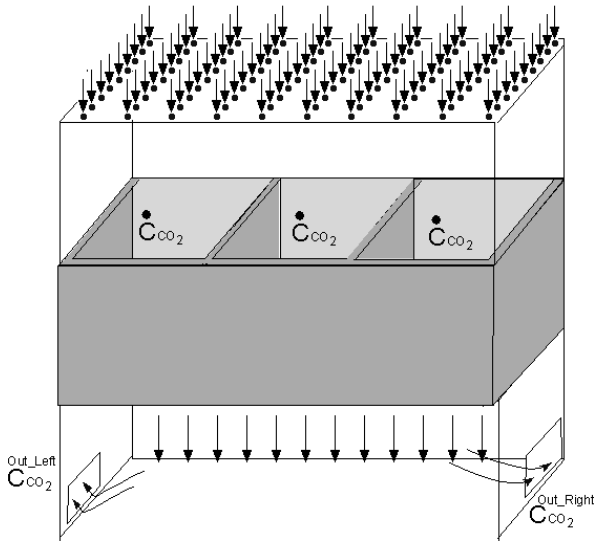

Figure 6 Sketch of the "cages ambient" and its boundary conditions in terms of concentration

The numerical simulations have provided the 3D convective fields and the related concentration patterns up to the steady state. The simulations show that the concentration of the different species at the steady state is almost uniform (see Figs. 8). This could be expected since the Schmidt number is unit.

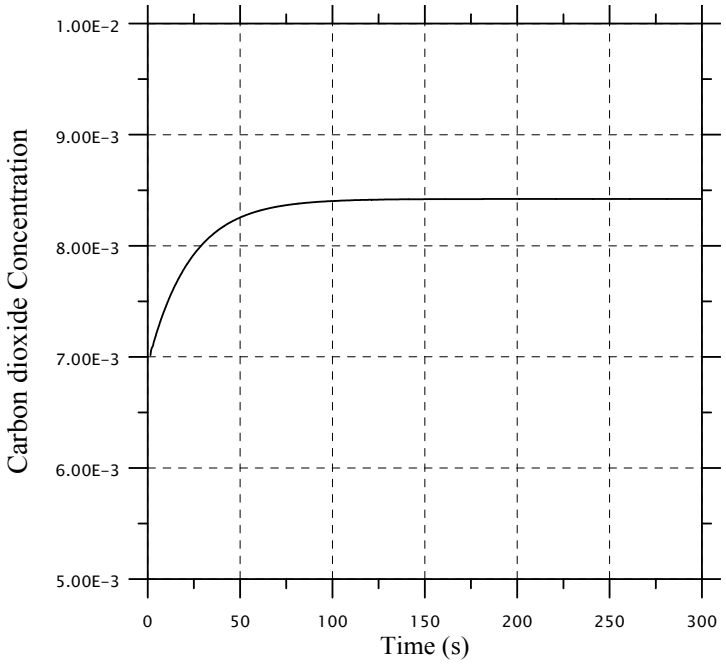

Figure 7 Average carbon dioxide concentration [%] as function of time

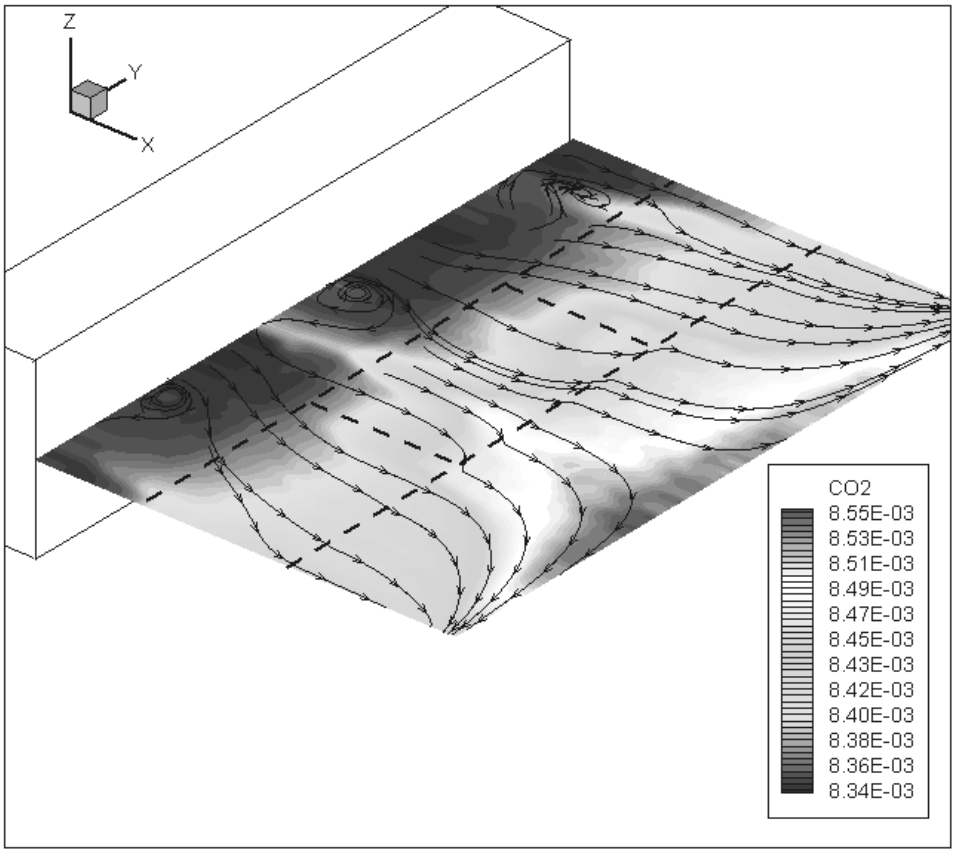

figure 8a: Carbon dioxide distribution [%] at the steady state in the midplane

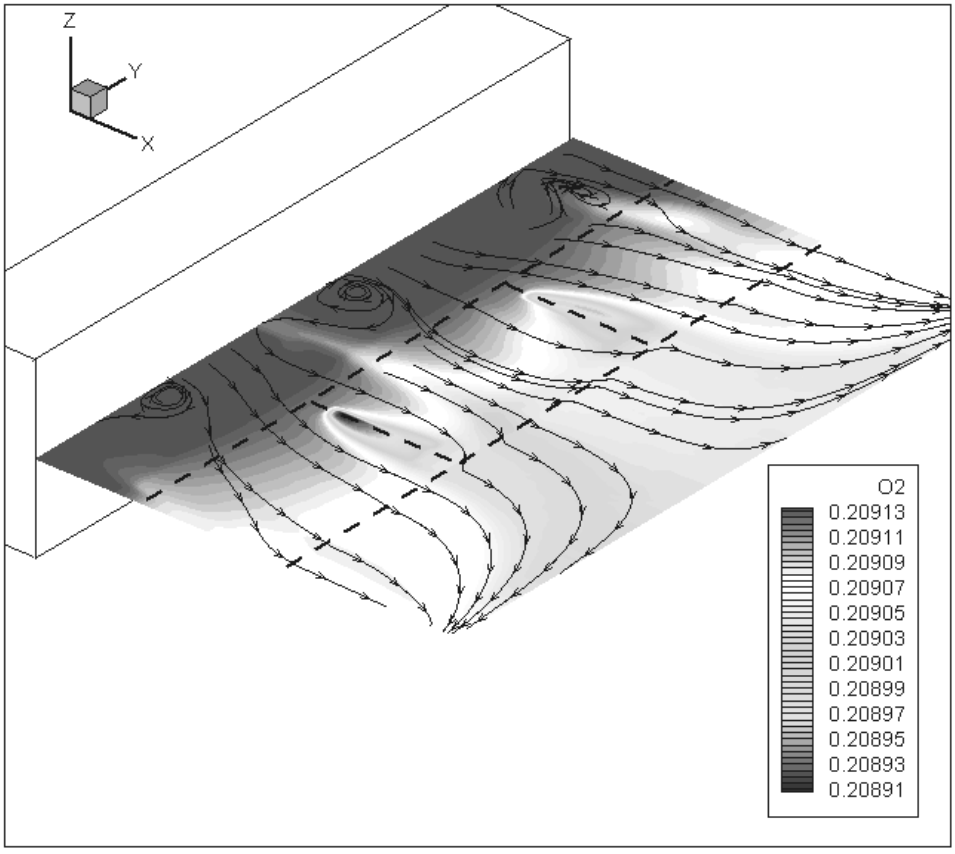

figure 8b: Oxygen distribution [%] at the steady state in the midplane

Due to the CO_2 mice production, the $C0_2$ concentration increases up to an average value of 0.84% (see Fig. 7) in the cages ambient (in cabin it is 0.7%). The level of O_2 is decreased from 21% (ISS value) to 20.9%. The steady state is reached after 150 [s].
The concentration of carbon dioxide tends to be larger (0.855%) in the regions behind the cages since there the velocity component along x tends to become small and the axial transport is less efficient. For the same reason, the concentration of oxygen tends to be lower therein (20.89%).

7. CONCLUSIONS

The MDS is a miniature laboratory animal facility that contains all of the components that are required for maintenance of the animals during a space-ISS-mission. The environment that will be provided by this System has been investigated through direct solution of the Navier-Stokes and species balance equations. The problem, being a very challenging task, has required the application and the "matching" of various numerical techniques such as the "porosity" approach and the volume of fraction method as well as very dense computational meshes. A "custom" model has been introduced to take into account all the different aspects of the problem under investigation.
The simulations have been carried out to match the requirements for the comfort and well-being of the animals (velocity and direction of the fluid in the cages, oxygen and carbon dioxide levels at the steady state, etc.).
The streamlines are almost parallel and the flow is almost uniform through the cages even if some complex patterns and vortical structures arise in other regions. The uniformity of the flow in the cages prevents the accumulation of impurities. The carbon dioxide and oxygen levels are tolerable throughout the system.

8. ACKNOWLEDGEMENTS

The authors would like to thank ASI for the financial support.

9. REFERENCES

[1] R.W. Ballard and R.C. Mains editors (1990), "Fundamentals of Space Biology", M. Asashima and G. M. Malacinski, eds. Springer-Verlag: New York , pp. 21-41.
[2] K. Souza, R. Hogan, and R. Ballard, editors (1993), "Life Into Space - Space Life Sciences Experiments - 25 Years: 1965-1990" (Comments Edition), NASA Ames Research Center: Moffett Field, CA, pp. 29-89.
[3] S. C. Cowin, "Bone stress adaptation models", Journal of Biomechanical Engineering, 115, (1993), 528-533.
[4] D. P. Fyhrie, M. B. Shaffler, "The adaptation of bone apparent density to applied load". Journal of Biomechanics, 28, (1995), 135-146.
[5] L. Taber, "Biomechanics of growth, remodeling, and morphogenesis", Applied Mechanics Review, 48, (1995), 487-545.
[6] R. D. Lange, L. A. Gibson, T. B. Driscoll, Z. Alleban , A. T. Ichiki, "Effects of microgravity and increased gravity on bone marrow of rats", Aviation and Space Environmental Medicine 65, (1994), 730-35.
[7] V. Cotronei, J. Sabbagh, R. Cancedda, G. Falcetti, L. Lunetta, "Mice Drawer System", Proceedings of the 2nd European Symposium on the Utilization of the International Space Station, ESTEC, Noordwijk, The Netherlands, 16-18 November 1998 (ESA SP-433, February 1999, pp. 449-454).
[8] H. B. Awbi, "Application of Computational Fluid Dynamics in Room Ventilation," Building and Environment, 24, (1989), 73-84.
[9] Q. Chen, A. Moser, P. Suter, "A Numerical Study of Indoor Air Quality and Thermal Comfort Under Six Kinds of Air Diffusion," *ASHRAE,.*98, Part 1, (1992), 203-217.
[10] Y. Li, "Simulation of Flow and Heat Transfer in Ventilated Rooms," Transactions of the Department of Mechanics/Applied Computational Fluid Dynamics, Royal Institute of Technology, S-100 44 Stockholm, Sweden, August 1992.
[11] J. L. Lage, A. Bejan, R. Anderson, "Removal of contaminant generated by a discrete source in a slot ventilated enclosure," Int. J. Heat Mass Transfer, 35 (5), (1992), 1169-1180.
[12] G. Gan, H. B. Awbi, D. J. Croome, "CFD Simulation of the Indoor Environment for Ventilation Design," *ASME Winter Annual Meeting, Transport Phenomena in Indoor Environmen*t, Paper 93, November 28 - December 3 1993, New Orleans, USA.
[13] G. Gan, H. B. Awbi, "Numerical Prediction of the Age of Air in Ventilated Rooms," *Procedure of the Fourth International Conference on Air Distribution in Rooms (ROOMVENT'94*), 15 - 17 June 1994, Cracow, Poland, Vol.2, pp.15-27.
[14] F. H. Harlow, J. E. Welch, 'Numerical calculation of time-dependent viscous incompressible flow with free surface", Phys. Fluids, 8, (1965), 2182-2189.
[15] V. R. Voller, C. Prakash, 'A fixed grid numerical modelling methodology for convection-diffusion mushy region phase-change problems', Int. J. Heat Mass Transfer, 30 (8), (1987), 1709-1719.
[16] W. D. Bennon, F. P. Incropera, 'A continuum model for momentum, heat and species transport in binary solid-liquid phase change systems-I. Model formulation', Int. J. Heat Mass Transfer, 30 (10), (1987), 2161-2170.
[17] A. D. Brent, V. R. Voller, J. Reid, 'Enthalpy-porosity technique for modelling convection-diffusion phase change: application to the melting of a pure metal', Num. Heat Transf., 13, (1988), 297-318.
[18] M. Lappa, "Strategies for parallelizing the three-dimensional Navier-Stokes equations on the Cray T3E "; Science and Supercomputing at CINECA, 11, (1997), 326-340.
[19] R. Savino, M. Lappa, D. Paterna, "Experimental and numerical analysis of three-dimensional surface tension and buoyancy-driven flows in cavities.", MSSU (Microgravity and Space Station Utilization), 2 (1), (2001), 13-22.
[20] M. Lappa, "Three-dimensional numerical simulation of Marangoni flow instabilities in floating

zones laterally heated by an equatorial ring", Phys. Fluids 15 (3), (2003), 776-789.
[21] C. W. Hirt, B. D. Nichols, 'Volume of Fluid (VOF) Method for the Dynamics of Free Boundaries', J. Comput. Phys., 39, (1981), 201-225.
[22] D. Gueyffier, J. Li, A. Nadim, S. Scardovelli, S. Zaleski, 'Volume of Fluid interface tracking with smoothed surface stress methods for three-dimensional flows', J. Comput. Phys., 152, (1999), 423-456.

Table I: discretization of the computational domain

	Nx	Ny	Nz
Diffuser system	42	208	58
Cages system	102	208	58

Table II: Properties and operating conditions

D_{O_2} [$cm^2\ s^{-1}$]	0.206
D_{CO_2} [$cm^2\ s^{-1}$]	0.164
ν_{air} [$cm^2\ s^{-1}$]	$1.567 \cdot 10^{-1}$
ρ_{air} [$g\ cm^{-3}$]	$1.225 \cdot 10^{-3}$
$A_{Filter1}$ [$N\ s\ cm^{-4}$]	$1.43 \cdot 10^{-4}$
$A_{Filter2}$ [$N\ s\ cm^{-4}$]	$1.43 \cdot 10^{-4}$
$Sc_{O_2} = \nu_{air} / D_{O_2}$ [-]	0.748
$Sc_{CO_2} = \nu_{air} / D_{CO_2}$ [-]	0.940
$\dot{C}_{O_2}$ [$cm^3\ s^{-1}$]	-0.3137
$\dot{C}_{CO_2}$ [$cm^3\ s^{-1}$]	0.2824
$C_{O_2}^{ext}$ [%]	21
$C_{CO_2}^{ext}$ [%]	0.7
$\dot{m}_{fan}$ [$cm^3\ s^{-1}$]	$8 \cdot 10^3$
$\dot{m}_{iss}$ [$cm^3\ s^{-1}$]	$2.8 \cdot 10^2$